IOP Publishing Phys. Med. Biol. 65 (2020) 035005 (12pp) https://doi.org/10.1088/1361-6560/ab63b5

Physics in Medicine & Biology

IPEM Institute of Physics and Engineering in Medicine

PAPER

Investigating neutron activated contrast agent imaging for tumor localization in proton therapy: a feasibility study for proton neutron gamma-x detection (PNGXD)

RECEIVED
7 July 2019

REVISED
4 December 2019

ACCEPTED FOR PUBLICATION
18 December 2019

PUBLISHED
24 January 2020

Kurt W Van Delinder[1,4], Daniel Crawford[1], Tiezhi Zhang[2], Rao Khan[2,3] and James L Gräfe[1,3]

[1] Department of Physics, Faculty of Science, Ryerson University, 350 Victoria St., Toronto, Ontario M5B 2K3, Canada
[2] Department of Radiation Oncology, Washington University School of Medicine, 660 S Euclid Ave, St Louis, MO 63110, United States of America
[3] Senior authorship is shared between these individuals.
[4] Author to whom any correspondence should be addressed.

E-mail: kvandelinder@ryerson.ca

Keywords: proton therapy, particle imaging, proton neutron gamma detection, gadolinium neutron capture, spectroscopy, Monte Carlo simulation

Abstract

Proton neutron gamma-x detection (PNGXD) is a novel imaging concept being investigated for tumor localization during proton therapy that uses secondary neutron interactions with a gadolinium contrast agent (GDCA) to produce characteristic photons within the 40–200 keV energy region. The purpose of this study is to experimentally investigate the feasibility of implementing this procedure by performing experimental measurements on a passive double scattering proton treatment unit. Five experimental measurements were performed with varying concentrations and irradiation conditions. Photon spectra were measured with a 25 mm^2, 1 mm thick uncollimated X-123 CdTe spectrometer. For a 10.4 Gy administration on a 100 ml volume phantom with 10 mg g^{-1} Gd solution placed in a water phantom, 1129 $\pm$ 184 K-shell Gd counts were detected. For an administered dose of 21 Gy and the same Gd solution measured in air, resulted in 3296 $\pm$ 256 counts. A total of 1094 $\pm$ 171, 421 $\pm$ 150 and 23 $\pm$ 141 K-shell Gd counts were measured for Gd concentrations of 10 mg g^{-1}, 1 mg g^{-1} and 0 mg g^{-1} for 7 Gy dose in air. The signal to noise ratio for these five measurements were: 7, 15, 6, 3, and 0.2, respectively. The spectrum contained 43 keV K_α and 49 keV K_β peaks, however a small amount of 79.5 and 181.9 keV prompt gamma rays were detected from gadolinium neutron capture. This discrepancy is due to a drop in the intrinsic detection efficiency of the CdTe spectrometer over this energy range. The measurements were compared with Monte-Carlo simulation to determine the contributions of Gd neutron capture from internal and external neutrons on a passive scattering proton therapy unit and to investigate the discrepancy in detected characteristic x-rays versus prompt gamma rays.

Introduction

The main advantage of proton therapy originates from the ability to deposit the maximum amount of dose to the prescribed volume, while sparing the healthy tissues beyond the range. As almost all treatment sites are routinely being treated with protons, a concern with remaining uncertainties threaten to compromise the primary benefit of treating with protons in the first place. These concerns can be generalized as an inability to accurately determine the clinical proton beam range, a need for better anatomical tumor localization and a lacking in the implementation of adaptive treatment techniques (Herring *et al* 1971, Keall *et al* 2001, Yang *et al* 2010, Paganetti *et al* 2012). Treatment planning often deals with these uncertainties by assuming an uncertainty in the proton beam range of 2.5%–3.5% plus an additional range margin of 1–3 mm (Paganetti 2012) to the clinical target volume (CTV).

Many new research solutions have been proposed to address the current limitations with proton therapy. One solution involves using positron emission tomography (PET) to detect the annihilation photons produced from

positron emitting isotopes formed as a byproduct of proton therapy. A few clinical studies have demonstrated the ability to determine mm range verification in favorable treatment circumstances (Knopf *et al* 2011). There are various limitations that are currently being investigated, but a main drawback is from low counting statistics, biological washout from particular treatment sites, and the location of a PET detection system in relation to the proton beam-line (Parodi *et al* 2007, Knopf *et al* 2009). Another promising solution, prompt gamma imaging involves the detection of secondary radiation produced by nuclear interactions in tissue from the incident proton beam. Directly with treatment, a wide spectrum of prompt gamma rays are produced from carbon, nitrogen and oxygen, which can be used for the determination of the proton beam range. Experimental studies have referenced the capability to determine the proton beam range to an accuracy of 2 mm (Draeger *et al* 2018, Krimmer *et al* 2018). The short-comings of this technique are the requirements for a detector with high efficiency over a broad energy range, spatial resolution and the ability to minimize scatter from both photons and neutrons (Polf *et al* 2009, Kim *et al* 2009).

Recently, a novel imaging procedure termed proton neutron gamma-x detection (PNGXD) was proposed as a potential solution that could be used solely or adjunct to another method. The premise of PNGXD is to take advantage of the secondary neutrons produced from the treatment unit and within the patient by capturing them using a pre-administered gadolinium contrast agent (GDCA) located within the tumor volume of interest (Gräfe 2017). Gadolinium, naturally abundant as seven isotopes, is comprised of ^{155}Gd (14.8% abundance) and ^{157}Gd (15.65% abundance) which have thermal neutron capture cross sections of 60 900 barns and 254 000 barns, respectively. As a result of this huge cross section, a GDCA injected tumor strongly favors a capture event. Following a gadolinium neutron capture event, 43 keV (K_α) and 49 keV (K_β) characteristic x-rays, and 79.5 keV, 181.9 keV gamma-rays are the main spectral photon energies produced. The two prompt gamma rays are a result of the thermal neutron capture with ^{157}Gd emitted from an excited state of ^{158}Gd$*$. The characteristic x-rays are emitted as a result of an electronic transition after a competing internal conversion interaction (Gräfe *et al* 2012). These photon energies are an optimal match for most standard nuclear medicine spectroscopic detectors. The gamma-rays and x-rays, like in prompt gamma imaging, are emitted instantaneously (within 10^{-9} s to 10^{-12} s).

Still lacking experimental study, prospective applications for this new imaging modality include the production of a tumor image, displayed in coincidence to therapeutic treatment. This dynamic image when fused with an anatomical modality such as CT or MRI, may produce a method to track tumor position. A logical step would be to synchronize the tumor image with adaptive therapy techniques, which would allow the benefit of further treatment customization. A prospective work-flow for integrating the PNGXD imaging procedure into the clinic can be seen within figure 1. In addition, gadolinium has been investigated as a neutron capture agent for neutron therapy, and recently has been investigated as a neutron capture agent for therapy using secondary neutrons from charged particle therapy (Safavi-Naeini *et al* 2018). The method proposed in this current research could be used to image the secondary dose enhancement from neutron capture reactions with gadolinium.

With the appeal of PNGXD concept being clinically used as a prospective proton therapy imaging procedure, a great deal of experimental validation is required. The initial study first proposing PNGXD focused on investigating the numerical scale of Gd interactions by a means of Monte Carlo simulation. Simulations were performed within Monte Carlo N-Particle (MCNP) version 6 using simple geometrical shapes. The number of Gd neutron captures per source proton were determined to be relevant in magnitude to produce a medical image (Gräfe 2017). In addition, a theoretical calculation for the number of characteristic x-rays produced for a standard spread out Bragg peak (SOBP) in water phantom demonstrated clinical potential. The next logical step is to further this study by performing experimental measurements using a clinical double scattering passive proton treatment unit with Gd solution of varied concentration and geometry. We performed measurements for different experimental setups on a Mevion S250 passive scattering treatment unit (Mevion Medical Systems, Inc., Littleton, MA, S250-0001). The experiments were also performed with Gd solution in a water phantom to mimic a tumor within a human body.

We compared our results with Monte-Carlo simulation to observe the contributions of Gd neutron capture resulting from internal and external neutrons. In addition, these simulations were used as a secondary validation for Gd characteristic counts as the measured spectra were quite noisy in the higher energy prompt gamma ray regions due to low detection efficiency in these energy regions.

Material and methods

Experimental measurements

All irradiations were performed with a Mevion S250 clinical proton therapy treatment unit (S250, Mevion Medical Systems, Littleton, MA). The Mevion S250 is a passive double scattering system, which uses two scatterers within the treatment gantry to produce a flat dose distribution. The Mevion S250 uses a 9 Tesla superconducting magnet to produce a 250 MeV proton beam using a compact synchrocyclotron (Cheng *et al* 2016). The treatment unit offers 24 different beam configurations organized into large, deep and small groups. The maximum achievable field size is 25×25 cm^2 with a greatest possible depth of 32 cm (Prusator *et al* 2018).

Table 1. Experimental geometries for the irradiation of a Gd solution on a Mevion S250 unit.

Experimental geometries	Gd concentration (mg g^{-1})	Dose (Gy)	Monitor units (MU)	Monitor unit rate (MU min^{-1})
1	10	10.4	1000	97
2	10	21.0	3000	124
3	10	7.0	1000	124
4	1	7.0	1000	124
5	0	7.0	1000	124

The experimental photon spectra were measured for five different conditions as listed in table 1. All experimental setups were located at 42 cm distance from the end of the nozzle to isocenter. There was no compensator used while a standard aperture was used to deliver $10 \times 10\,cm^2$ field size. Geometry 1 was performed on a $30 \times 30 \times 30\,cm^3$ PTW water phantom, which had 1 cm thick acrylic walls. All experimental measurements involved gadolinium solution in a 100 ml Nalgene bottle with height to diameter of 7.5 cm × 4.9 cm. The solution height in the bottle was 5.7 cm. The delivered dose is shown in table 1. Due to the beamline design, the output factors (cGy/MU) of double-scattering proton beams (cGy/MU) are not the same for different options. We estimated the output factors based on an empirical model developed by Kooy *et al* (2005) at the Massachusetts General Hospitals (MGH) and then calculated dose based on total MU delivered. In this model, the output factor was modeled as a function of combined parameters of range (R), modulation width (M) and source shift changes based on measurement data. The predicated values are mostly within 3% of the measured values based on our clinical measurements, thus is sufficient for this study.

All spectroscopic measurements were performed using an Amptek X-123 CdTe (Amptek, Bedford, MA, X016037) uncollimated spectrometer with a $25\,mm^2$ surface area and a thickness of 1 mm. The measured energy bins ranged from 12.96 to 259.27 keV and were divided into 8192 channels. The spectra were acquired using the Amptek DPPMCA Display & Acquisition Software version 1.0.0.20 (Amptek, Bedford, MA). We calibrated the detector with ^{241}Am and ^{57}Co calibration sources. The detector dead-time was recorded for each experimental geometry.

Borated polyethylene (BPE) with a total thickness of 5 cm was used for shielding the front, top and bottom sides of the detector, while a 2.5 cm sheet was placed at the back far side from the treatment head (see figure 2). Geometry 1, in water phantom, consisted of a 4.5–9.5 cm SOBP while geometries 2–5 all used a consistent range of 0–5 cm SOBP. Geometries 2 through 5 all maintain the exact same distances with respect to the treatment nozzle and detector; only the concentration of gadolinium or delivered dose was varied.

For in-phantom measurements, the center of the gadolinium bottle was placed at a distal depth of 7 cm in water phantom, effectively at 8 cm depth with the acrylic walls included. A lateral distance of 3.8 cm from the center of solution was used within water phantom, effectively at 4.8 cm including the phantom walls. The detector was positioned 10 cm away from the wall of the water tank. The same detector distance of 10 cm was used for the in-air measurements. The detector surface, indicated by a red guard (figure 2) is used for all geometrical distances, however, the actual CdTe detector crystal is located approximately 1 mm behind the guard.

Experimental fittings

The experimental peaks were fitted using standard Gaussian functions within OriginPro 2018 (OriginLab, Northampton, MA). The noisy higher energy spectral regions which contained the 79.5 keV and 181.9 keV Gd prompt gamma rays were smoothed by applying Savitzky–Golay smoothing functions. A reduced-chi square value of approximately 1.0 was consistently achieved throughout each of the experimental fittings.

Each of the characteristic photons and gamma-rays were individually fit with an uncertainty due to a unique background over each region. For gadolinium, the $K_{\alpha 1}$ and $K_{\alpha 2}$ peaks are 42.3 keV and 43 keV, respectively. Therefore, the sum of both peaks are quantified for the total K_α values. For both noisy 79.5 keV and 181.9 keV peak regions, nearby peaks were also fit to distinguish between local peaks. It must be mentioned that the CdTe detector has a manufacturer specified 1.5 keV energy resolution at 122 keV, therefore closely located peaks may not be easily distinguishable.

CdTe detection efficiency

To validate the CdTe detector modelling in MCNP6 (Goorley *et al* 2012), the absolute detection efficiency (DE) was experimentally quantified and compared to simulations. The experimental measurement was performed using two radioactive isotopes, ^{133}Ba (30.8, 35, 80 keV), and ^{57}Co (122 keV) placed 4.67 cm away from the detector end-cap. The CdTe detector including the 0.075 cm Be window were modeled in MCNP6. Isotropic point sources at the same distance as the experimental geometries were modelled at each of the photon energies. The F8 tally energy distribution of pulses was measured as 1 keV bins from 0 to 250 keV for 50 million photons.

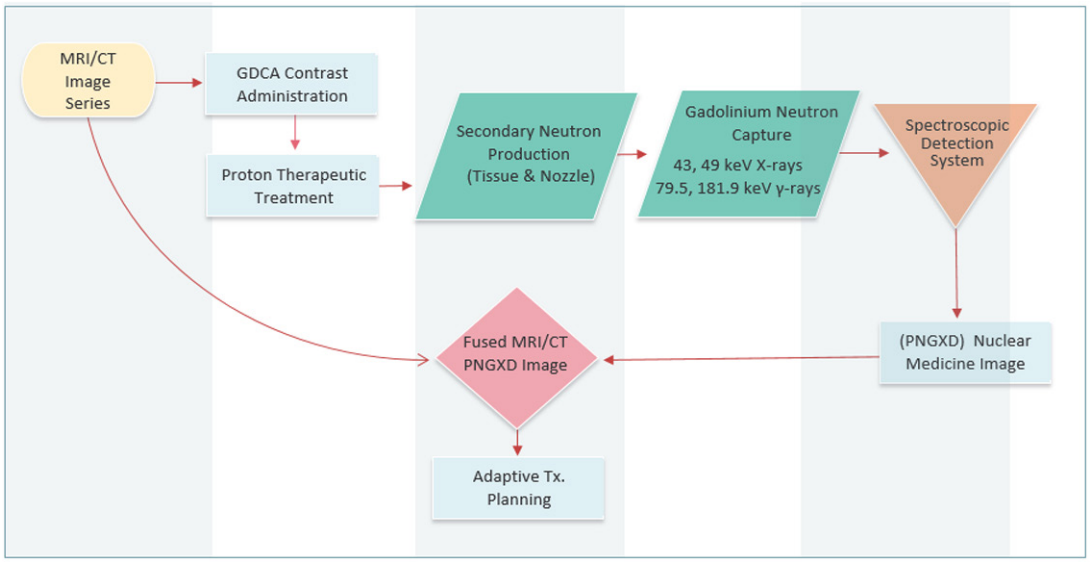

Figure 1. Clinical work-flow demonstrating the process of integrating the PNGXD imaging procedure. The acquired nuclear medicine image is intended to be fused directly with an anatomical imaging modality (CT/MRI). The possibility to correlate this imaging modality with adaptive techniques may be attainable.

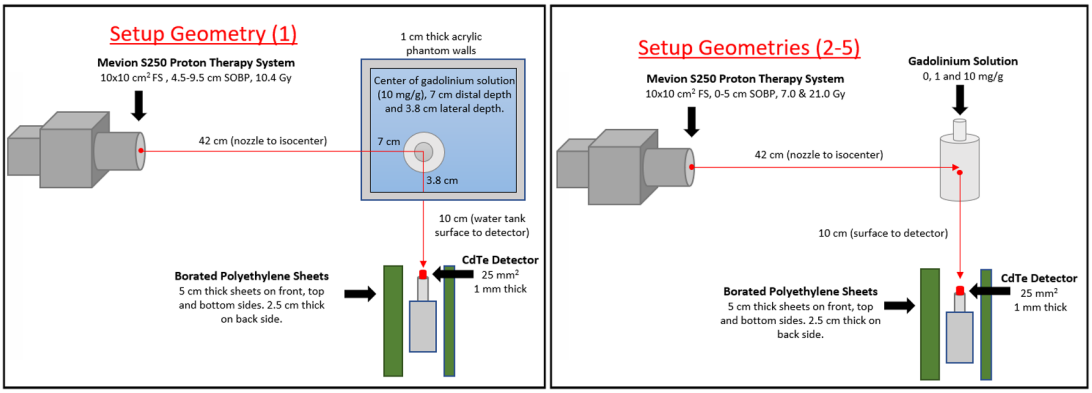

Figure 2. Setup diagrams for each experimental geometry. The dimensions for each geometry including the placements of the treatment nozzle, gadolinium solution, detector and respective geometrical distances are listed in the diagram.

The quantified statistical uncertainty was much lower than 1% per energy bin. All MCNP6 default cut values were used for all particles, which is equivalent to a cutoff energy of 0.001 MeV for both electrons and photons.

MCNP simulations

MCNP—proton treatment model

A simple model of the proton treatment conditions was created. The treatment head components were not modelled as we were only interested in comparing experimental trends with Monte Carlo simulation. To assess the experimentally measured results, conditions 1 and 2 were modelled in MCNP replicating the same geometrical distances as can be seen in figure 2. To model the proton component a $10 \times 10\,\text{cm}^2$ field size planar proton beam was created at a distance of 42 cm to the center of the Gd solution or SOBP isocenter within water phantom. The spread-out Bragg peak (SOBP) was modelled using a formalism (Jette *et al* 2011) that uses an energy weighted distribution replicating the SOBP. Both conditions used a p-value of 1.66, which is defined in Jette and Chen (2011) and relates the range of protons to their energy. We used 50 energy bins to create the SOBP.

The 4.5–9.5 cm and 0–5 cm SOBPs, have energy ranges from 75–113 and 9–78 MeV, respectively. The SOBP distributions were validated by running the weighted energy distributions on a water phantom and measuring the dose deposition.

MCNP—neutron treatment model

Since all of the components in the machine were not modelled, creating a neutron source from the treatment unit is not possible. Instead, we resorted to using the published data by Chen *et al* (2013). To produce the neutron

component from a Mevion S250 treatment nozzle, the neutron output of configuration B, position 1 from Chen *et al* (2013) was replicated. The 10 cm SOBP was first produced using the formalism described above. The effective source was located −42 cm to isocenter for both proton and neutron beams from a water phantom with dimensions of 68 cm depth, 40.7 cm height, and 35 cm width. The proton dose was calculated within a $2 \times 2 \times 2\,cm^3$ box using the F6 tally located at the center of the SOBP.

To replicate the neutron source output, data from a plot of neutron fluence versus energy Chen *et al* (2013) was extracted using a data extractor. The spectral distribution was then transferred as an isotropic neutron source with the same energy weights. The neutron dose was then calculated using the F4 tally fluence measurement along with the ICRP 74 fluence-to-dose equivalent conversion factors (ICRP 1996). As in the work of Chen *et al* (2013) this was scored within a 6 cm radius air-filled sphere located 100 cm away from the proton beam isocenter. We then scaled the neutron component to match the same mSv neutron/Gy proton measured by Chen *et al* (2013).

MCNP—experimental simulations

For both in phantom and in-air geometries, the proton and neutron sources were simulated individually in two separate runs and combined since MCNP does not allow running multiple sources of different particles at once. The statistical uncertainty in all tally results was kept below 2%. Materials were largely defined using the MCNP6 continuous-energy neutron data libraries using the most recent ENDF material card. Thermal S(α,β) cross-section libraries were used for the water component of the gadolinium solution and water phantom. Endf70prot proton data libraries were used when available, otherwise the default cascade-exciton model (CEM) was used for proton simulations. For all simulations, the proton dose was calculated over the gadolinium solution using the F6 Tally. To calculate the number of neutron captures produced in solution, the FM tally multiplier was used and scaled as given by equation (1). An (n, γ) ENDF reaction number was added to this tally multiplier to integrate the neutron fluence over the energy dependent neutron capture cross section. Equation (1), shows the devised formalism to calculate the amount of photons detected in the CdTe detector scaled by emission probability of the corresponding gamma or x-ray resulting from neutron capture:

$$\frac{\text{Detected}}{\text{Gy}} = \left(\frac{n}{\text{Gy}}\right)(\text{DE})(\Gamma)(N_t)(I_{AB})(\text{Gd}_{\text{Conc }(\%)})(T_M). \quad (1)$$

Where Gy/n is the dose per neutron measured for each geometry over the entire gadolinium solution volume, DE is the detection efficiency of each experimental geometry with the simulated photon energy, Γ is the gadolinium x-ray or prompt gamma ray emission probability, N_t is the number of Gd target atoms, I_{AB} is the ^{157}Gd isotopic abundance, $\text{Gd}_{\text{Conc }(\%)}$ is the gadolinium concentration in the solution, T_M is the MCNP6 Tally Multiplier output which represents the number of neutron capture events with ^{157}Gd.

Results

CdTe detection efficiency

The absolute detection efficiency of the CdTe detector, defined as the number of photon counts detected divided by the number of photons emitted are shown in figure 3.

The percentage difference between simulation and experiment for the selected energies of interest, 30.8, 35, 80 and 122 keV were quantified to be 8%, 9%, 4.5% and 16%, respectively. The difference can be attributed to the simplified modelling of the source and detector geometry. A trend of the simulated DE being higher than the experiment can be observed and is consistent throughout all measurements. This is most likely due to slight differences in the detector crystal position behind the Be window. The percent differences between the experiment and simulation are to be considered when assessing the PNGXD simulated results. The detection efficiencies for the characteristic Gd photons were determined by simulating each experimental setup and using a volume source from the gadolinium solution. The F8 pulse height tally was set to the CdTe detector and binned from 0 to 250 keV in 1 keV energy bins. The results are shown in table 2 along with photon emission probabilities.

Experimental measurements

The measurement results for geometry 1 can be viewed in figure 4. The K_α peaks are clearly visible, however the prompt gamma rays of 79.5 keV and 181.9 keV are hard to distinguish from the background. For a total of 10.4 Gy, 10 mg g^{-1} Gd concentration in water phantom 871 ± 163, 43 keV K_α photons and 258 ± 86, 49 keV K_β photons were measured. With the fitting, 70 ± 59 counts at 181.9 keV γ-rays and 521 ± 159 counts at 79.5 keV γ-rays were determined. This geometry is similar to a planar proton beam incident on human tissue. The relative detection efficiency drops by a factor of 0.84 and 0.22 when comparing the 79.5 keV and 181.9 keV regions to the 43 keV region.

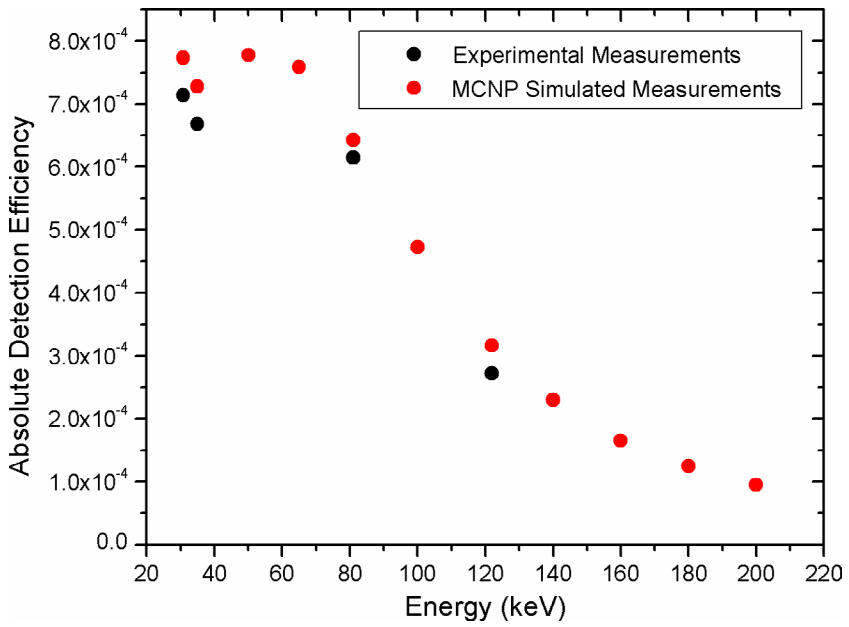

Figure 3. Absolute detection efficiency comparison between experiment and simulation.

Table 2. Absolute detection efficiencies of the characteristic Gd photons modelled for geometries 1 and 2 within MCNP6.

	Experimental geometry 1		Experimental geometry 2	
Emission probability	Photon energy (keV)	Absolute detection efficiency	Photon energy (keV)	Absolute detection efficiency
[a]0.25	43	2.97×10^{-5}	43	7.15×10^{-5}
[b]0.1	79.5	3.22×10^{-5}	79.5	6.58×10^{-5}
[b]0.183	181.9	7.44×10^{-6}	181.9	1.44×10^{-5}

[a] K_α emission probability per neutron capture with Gd from Gräfe *et al* (2012).
[b] ^{157}Gd γ-ray emission probabilities per neutron capture from IAEA (2006).

The entire labelled spectrum from geometry 2 can be observed within figure 5. The experimental fitted results for geometry 2 are displayed in figure 6, where 21.0 Gy dose was delivered to the Gd solution without a water phantom. A fitted value of 2597 ± 227 for 43 keV (K_α) and 699 ± 119 for 49 keV (K_β) Gd characteristic x-rays were measured. A count of 301 ± 80, 181.9 keV γ-rays and 1008 ± 133, 79.5 keV γ-rays were fitted. The prompt gamma rays could be measured above background in this geometry at roughly the correct proportions with respect to the 43 keV x-rays when emission probabilities and detection efficiencies are taken into account. This experiment resulted in the highest signal due to the fact that there was no additional attenuation of the water phantom and this resulted in the closest phantom to detector distance.

Figure 7 demonstrates the variation in signal counts from the same geometry as geometry 2 but with a different dose and gadolinium concentration. A direct correlation between signal counts and a decrease in dose from geometry 2 to geometry 3 can be observed. Similarly, the trend in signal with variation in gadolinium concentration can be established and it should be noted that Gd was not detectable in the zero concentration phantom. Based on linear extrapolation the ratio of counts from geometry 3 to geometry 4 should be a factor of 10 as the only thing that changes is a decrease in Gd concentration from 10 mg g^{-1} to 1 mg g^{-1}. However, it is well known that there is a non-linear response due to the enormous neutron capture cross section of Gd which leads to self-shielding and fluence suppression phenomena (Gräfe *et al* 2010, Gräfe 2017). Based on previous work the expected ratio is 2.7 (Gräfe 2017), which is in agreement with the value of 3.0 ± 1.6 measured experimentally (see table 3). This provides further evidence that the measured counts are from neutron capture reactions with Gd.

The total fitted counts for all characteristic x-rays and γ-rays are displayed within table 3. From the previously calculated detection efficiencies, the amount of characteristic photons emitted from the gadolinium solution can be approximated by using the experimentally detected values and solving for the number of photons emitted. From this method, a value of 3.3×10^7 and 4.5×10^7 43 keV K_α photons (dead-time corrected) for conditions 1 and 2 were estimated to be emitted from the solution, respectively. The signal-to-noise (SNR) ratios in table 3 were calculated by dividing the measured counts by the uncertainty from the signal fitting. The uncertainty from

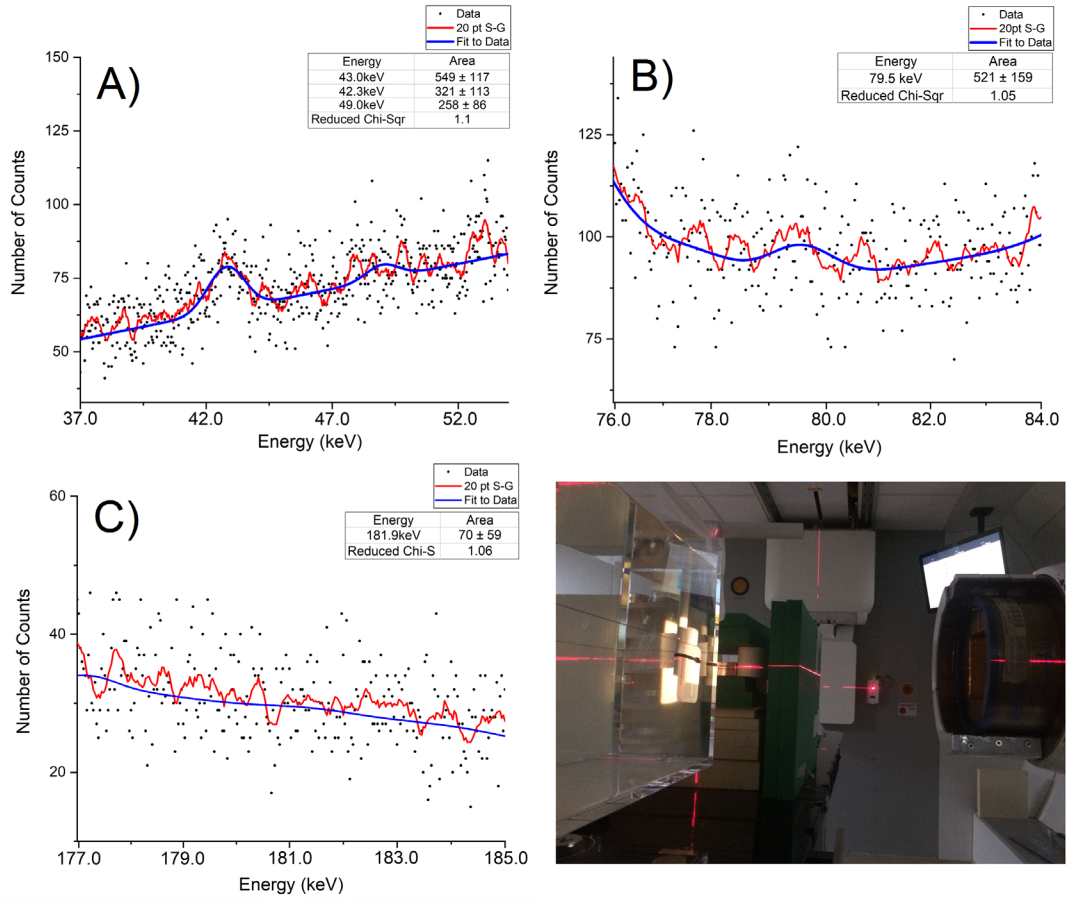

Figure 4. Raw fitted spectra for geometry 1 using 10 mg g^{-1} Gd solution at energies of (A) 43 and 49 keV (Gd characteristic x-rays) (B) 79.5 keV (prompt γ-rays) (C) 181.9 keV (prompt γ-ray) and (D) photo from geometry 1.

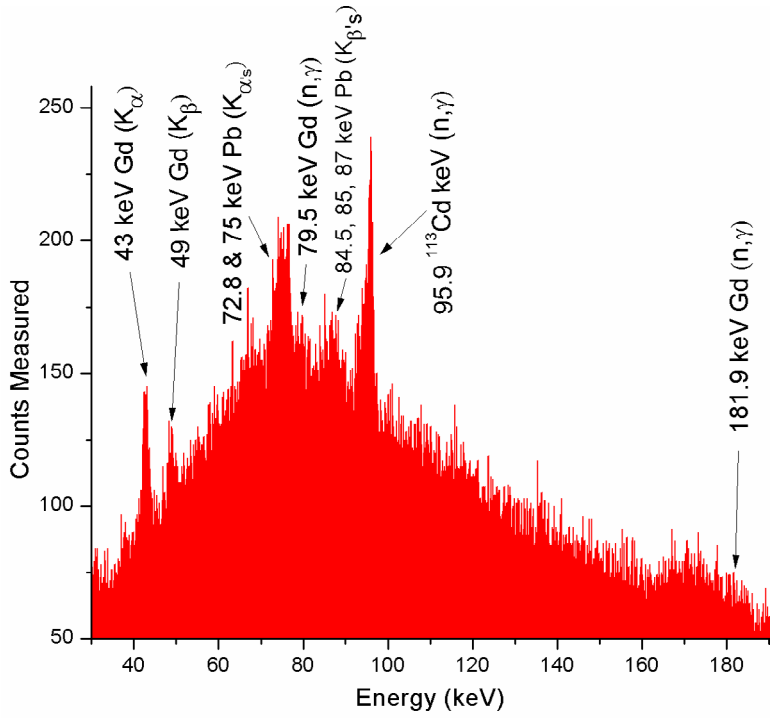

Figure 5. Raw labelled spectrum of identified peaks from geometry 2 measured with the CdTe detector.

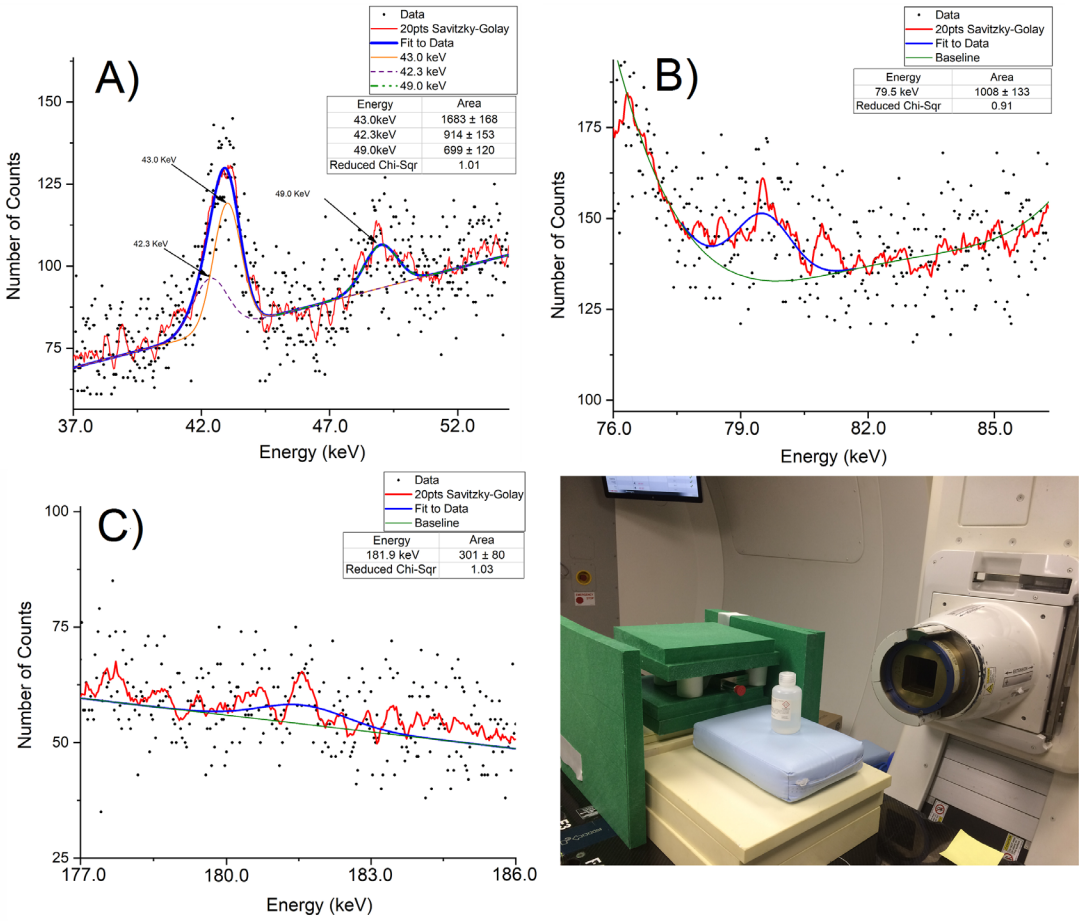

Figure 6. Raw fitted spectra for geometry 2 consisting of 10 mg g^{-1} Gd solution in water phantom. The energies fitted are (A) 43 keV and 49 keV (Gd characteristic x-rays) (B) 79.5 keV (prompt gamma-ray) (C) 181.5 keV (prompt gamma-ray) and (D) photo from geometry 2.

fitting includes the background signal as well as uncertainties from the fit in OriginPro, which uses the Levenberg Marquart non-linear fitting algorithm.

MCNP simulations

The MCNP6 simulation results from both the proton and neutron source simulation models are listed in table 4. The simulation results calculated from the amount of neutron capture in Gd were consistently higher than the experimental measurements for both simulations.

The largest number of photon counts was measured from the 43 keV x-ray emission and therefore is the best photon energy to analyze in order to reduce the effects of statistical uncertainty. The simulation and experimental measurements for this energy were compared, the predictions from MCNP were found to have 7.5 times more counts for geometry 1, and 1.4 times more for geometry 2. The high degree of disagreement for geometry 1 is hypothesized to be a result of both the method used for the neutron source modelling and the accuracy of the neutron production data libraries employed in simulation. The Mevion S250 passive double scattering neutron spectrum was modelled as one isotropic source scaled from a neutron spectrum produced by a fully-modelled treatment unit. This single source model approximates the treatment head neutron source as one component, however a dual source model neutron source may exhibit greater accuracy. A dual source neutron spectrum would consist of a setup dependent, low energy isotropic neutron source in addition to a more forward directed higher energy anisotropic neutron component. Secondly, the high ratio for geometry 1, is hypothesized to result from a large amount of neutron production within the simulated 30 × 30 × 30 cm^3 water phantom, originating from the high energy proton source incident and traversing the phantom. Regardless, the contribution of characteristic photons from the neutron and proton source models are almost equivalent for geometry 1 with a slightly larger contribution originating from the neutron source model. In the proton source model all neutrons are produced within the phantom, whereas in the neutron source model, we directly modelled the neutrons coming from the treatment head.

Geometry 2 consisted of irradiating the Gd solution directly without a water phantom. The contribution to Gd neutron capture is almost exclusively from the neutron source model that replicates the Mevion S250

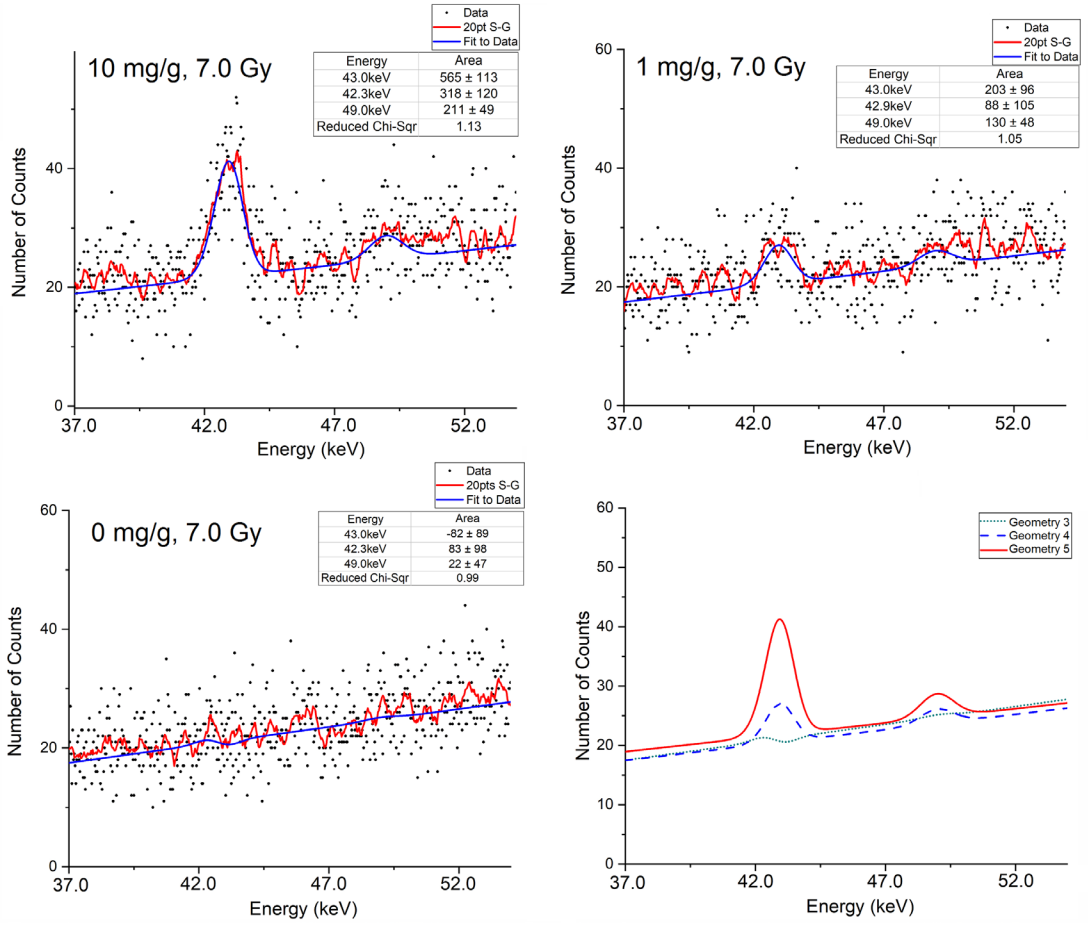

Figure 7. Fitted spectra for geometries 3, 4, and 5 consisting of the energies fitted for the 43 keV and 49 keV characteristic x-rays. The fourth image depicts all three geometries plotted onto one graph and their corresponding total fitting functions.

Table 3. Measured gadolinium characteristic x-rays and γ-rays tabulated for each of the experimental conditions. The measured counts were not corrected for dead-time.

	Experimental counts (keV)				
Geometries	43	49	79.5	181.9	SNR
1	871 ± 163	258 ± 86	521 ± 159	70 ± 59	7
2	2597 ± 227	699 ± 119	1008 ± 133	301 ± 80	15
3	883 ± 164	211 ± 49	N/D	N/D	6
4	291 ± 142	130 ± 48	N/D	N/D	3
5	0.9 ± 133	22 ± 47	N/D	N/D	0.2

N/D. Not detected. Peak was not experimentally fit for N/D listing due to a low number of counts.

treatment unit head components. Nevertheless, the simulation was able to predict the production and detection of Gd x-rays and γ-rays on the same order of magnitude as the experiment. We also see that depending on the irradiation site that the relative contribution to the signal from internally created neutrons (within the patient) and external neutrons (from the treatment head) will vary.

Discussion

The detected 79.5 and 181.9 keV γ-rays were much lower than the Gd characteristic x-rays despite being produced by the same neutron capture events. This is due to the large drop in detection efficiency over these higher energy regions, and the lower emission probabilities per neutron capture. The relative detection efficiency drops by a factor 0.84 and 0.22, for the 79.5 and 181.9 keV γ-rays, respectively, compared to the 43 keV K_α emission. For this particular detector, the number of γ-rays detected is too low to produce any meaningful contribution to a projected image. Due to this reason, a well-collimated detection system with an increased detection efficiency over this higher energy range is recommended for future studies. This can be accomplished by using a thicker

Table 4. MCNP6 tabulated count values calculated from the FM Tally multiplier and the gadolinium photon emission probabilities. The measured values were corrected for dead-time for comparison with simulation.

		Neutron Source	Proton source			
Geometries	Energy (keV)	MCNP6 counts	MCNP6 counts	MCNP6 total counts	Measured counts (CdTe)	Ratio (MCNP/ measured)
1	181.9	711	648	1359	79 ± 66	17.2
	79.5	1679	1532	3211	589 ± 180	5.5
	43	3881	3541	7422	984 ± 184	7.5
2	181.9	654	16	670	376 ± 100	1.8
	79.5	1634	40	1674	1260 ± 166	1.3
	43	4444	110	4554	3246 ± 284	1.4

CdTe detector. Alternatively, there are many different spectroscopic detectors that would be an ideal match: such as hyperpure germanium (HPGe) or thallium activated sodium iodide (NaI(Tl)).

Modelling the neutron production accurately from a passive scattering treatment unit is widely accepted as a very difficult task to accomplish (Agosteo *et al* 1998, Polf *et al* 2005, Zheng *et al* 2007, Moyers *et al* 2008, Chen *et al* 2013). To produce accurate results, it is recommended that full details of the treatment unit specifications are used in the model. These details are often proprietary. However even with these details, agreement between simulation and experiment is often difficult to achieve for the neutron components. Therefore, the decision to accurately model an output from a pre-validated simulation of the Mevion S250 was deemed appropriate for this work. The limitations of this method are that we are basing our measured outputs from a different setup configuration, which does not precisely match ours. As a result, the secondary neutron production within our exact components are not included. However, it has been determined by Chen *et al* (2013) that for this treatment model the measured secondary neutron fluence distribution has a relatively consistent spectral shape, even with variation in experimental setup. Therefore, the implementation of this method to extract the neutron spectral component from the treatment model head can be deemed valid as an approximation to the measured output from a fully modelled proton treatment unit.

From our experimental results, it was determined that in order to produce a large amount of Gd K-shell x-rays and gamma-ray counts, a high Gd concentration and a large administered proton dose is required. Previous studies have estimated that an upper limit of Gd absorption within a cancerous tumor is approximately 0.3 mg g^{-1} (Masiakowski *et al* 1992, Shih *et al* 1992, Culbertson *et al* 2003). Therefore, we can deduce that to obtain a high enough Gd signal, a large amount of dose administered within a small amount of fractions, as in stereotactic radiosurgery (SRS) or stereotactic body radiation therapy (SBRT), may be the only feasible method to clinically implement PNGXD. Stereotactic treatment techniques require additional quality assurance (QA) consideration and are greatly effected by the current uncertainty issues with proton therapy (Paganetti 2018). Consequently, the justification to implement an additional imaging procedure like PNGXD may be clinically warranted. More recently, researchers have been able to achieve an order of magnitude higher amount of Gd (3 mg g^{-1}) within T98G glioblastoma tumor cells (Morrison *et al* 2014). This would result in more favorable detection characteristics. In addition, direct administration of a GDCA during treatment could be investigated. In this situation the concentration of Gd would be expected to be significantly higher (Ahmad *et al* 2017). Alternatively, a GDCA enriched in the ^{157}Gd isotope could be investigated to increase the neutron capture rate. The PNGXD procedure would not only allow imaging of tumor contrast uptake but would also provide an image of the location of dose enhancement from neutron capture reactions within the tumor for Neutron Capture Enhanced Particle Therapy (NECPT) (Safavi-Naeini *et al* 2018). The technique was recently proposed by the authors of that study as an 'opportunistic' dose enhancement from neutrons produced in charged particle therapy and is based on the same premise as boron neutron capture therapy or gadolinium neutron capture therapy.

The current study investigates the first detection of Gd on a proton therapy treatment unit using a CdTe spectroscopic detector. As a novel imaging application, we propose to use the 43 and 49 keV K-shell photons in addition to the 79.5 and 181.9 keV prompt γ-rays from Gd to produce a nuclear medicine image. This discrete energy spectrum has an advantage in detection efficiency for most nuclear medicine detectors, when compared to imaging with secondary prompt gamma-rays in tissue which may reach as high as several MeV (Verburg *et al* 2014). The experimental measurements performed with an uncollimated small volume single pixel detector can be used to scale up to the number of counts on a much larger detection system for pre-clinical conceptual future studies. The signal-to-noise ratios for conditions 1 and 2 were determined to be greater than 5, which fulfills the Rose model criteria; a common metric in medical imaging to signify that an acceptable image can be produced.

From this study, it was determined that the total measured signal may be a limitation to imaging with PNGXD, however, there have been many scientific advances recently within the area of producing high quality medical

images by detecting only a small amount of photon counts (Wronski *et al* 2010, Taguchi *et al* 2013, Morris *et al* 2015, Zhu *et al* 2018). An acceptable SNR with low counting statistics may still produce a high-quality medical image (Morris *et al* 2015).

To further this investigation, the next study will be focused on simulating a full spectroscopic detection system with SPECT detectors. The detected photon counts from the experimental measurements of the current study can be back-calculated to the number of photons emitted from the Gd solution. This number of emitted photons can be added as a volume source within any organ or region of interest within a DICOM image. The simulation can be made to output a direct 2D image or a 3D reconstruction using the experimentally measured photon production rate. This can provide a good approximation to indicate whether or not a medical image of acceptable quality can be produced from PNGXD.

Conclusion

Experimental measurements were performed under various conditions from a passive scattering proton therapy treatment unit on a Gd solution to determine the feasibility of imaging tumor contrast agent distribution from secondary neutron capture reactions in particle therapy. Measurements were obtained on a 25 mm^2 single pixel CdTe detector. A total of 1129 $\pm$ 184 K-shell counts were detected for an administered 10.4 Gy on a 100 ml volume bottle of 10 mg g^{-1} Gd solution within a water phantom. For 21.0 Gy delivered on a 100 ml volume of 10 mg g^{-1} Gd without a water phantom, 3296 $\pm$ 256 K-shell counts were measured. A signal-to-noise ratio of greater than 5 was determined for both of these experimentally measured spectra positively indicating the potential to produce an image of a Gd contrast agent during proton therapy.

The results suggest that the percent of Gd absorbed within a clinical tumor and the requirement for the administration of a high dose fraction may limit this application to stereotactic treatment procedures for the current detector design. Further studies will focus on evaluating a full detection system with high geometric efficiency using the measured Gd photon production rate obtained from within this experimental study. This should provide further insight into the image quality produced from the proposed nuclear medicine imaging procedure for particle therapy.

Acknowledgments

This work is supported by the Natural Sciences and Engineering Research Council of Canada (NSERC) and by the Ryerson University Faculty of Science Dean's Research Fund.

ORCID iDs

Kurt W Van Delinder https://orcid.org/0000-0003-3776-3768
Rao Khan https://orcid.org/0000-0002-7373-6858
James L Gräfe https://orcid.org/0000-0001-8309-0088

References

Agosteo S, Birattari C, Caravaggio M, Silari M and Tosi G 1998 Secondary neutron and photon dose in proton therapy *Radiother. Oncol.* **48** 293–305

Ahmad S B, Paudel M R, Sarfehnia A, Kim A, Pang G, Ruschin M, Sahgal A and Keller B M 2017 The dosimetric impact of gadolinium-based contrast media in GBM brain patient plans for a MRI-Linac *Phys. Med. Biol.* **62** N362

Chen K L, Bloch C D, Hill P M and Klein E E 2013 Evaluation of neutron dose equivalent from the Mevion S250 proton accelerator: measurements and calculations *Phys. Med. Biol.* **58** 8709

Cheng C W, Ferguson S G, Jordan D, Jesseph F, Johnson M, Bouchet L, Mansur D and Wessels B 2016 Impact of the high magnetic field and RF power in a superconducting cyclotron on the operation of a nearby MRI facility *Proton Ther.* **2** 1–9

Culbertson C N and Jevremovic T 2003 Computational assessment of improved cell-kill by gadolinium-supplemented boron neutron capture therapy *Phys. Med. Biol.* **48** 3943

Draeger E, Mackin D, Peterson S, Chen H, Avery S, Beddar S and Polf J C 2018 3D prompt gamma imaging for proton beam range verification *Phys. Med. Biol.* **63** 035019

Goorley T *et al* 2012 Initial MCNP6 release overview *Nucl. Technol.* **180** 298–315

Gräfe J L 2017 Proton neutron gamma-X detection (PNGXD): an introduction to contrast agent detection during proton therapy via prompt gamma neutron activation *Nucl. Instrum. Methods Phys. Res.* B **407** 20–4

Gräfe J L, McNeill F E, Byun S H, Chettle D R and Noseworthy M D 2010 A benchmarked MCNP model of the *in vivo* detection of gadolinium by prompt gamma neutron activation analysis *Nucl. Instrum. Methods Phys. Res.* B **268** 2451–7

Gräfe J L, McNeill F E, Chettle D R and Byun S H 2012 Characteristic x ray emission in gadolinium following neutron capture as an improved method of *in vivo* measurement: a comparison between feasibility experiment and Monte–Carlo simulation *Nucl. Instrum. Methods Phys. Res.* B **281** 21–5

Herring D F 1971 The degree of precision required in the radiation dose delivered in cancer radiotherapy *Br. J. Radiol.* **5** 51–8

IAEA 2006 *Database of Prompt Gamma Rays from Slow Neutron Capture for Elemental Analysis* (Vienna: International Atomic Energy Agency)
ICRP 1996 ICRP Publication 74: Conversion coefficients for use in radiological protection against external radiation *Ann. ICRP* **26** 1–205
Jette D and Chen W 2011 Creating a spread-out Bragg peak in proton beams *Phys. Med. Biol.* **56** N131
Keall P J, Kini V R, Vedam S S and Mohan R 2001 Motion adaptive x-ray therapy: a feasibility study *Phys. Med. Biol.* **46** 1
Kim J W, Kubo H and Tanimori T 2009 Prompt gamma measurements for the verification of dose deposition in proton therapy *Medical Physics* vol 36 (Hoboken, NJ: Wiley)
Knopf A C, Parodi K, Paganetti H, Bortfeld T, Daartz J, Engelsman M, Liebsch N and Shih H 2011 Accuracy of proton beam range verification using post-treatment positron emission tomography/computed tomography as function of treatment site *Int. J. Radiat. Oncol. Biol. Phys.* **79** 297–304
Knopf A, Parodi K, Bortfeld T, Shih H A and Paganetti H 2009 Systematic analysis of biological and physical limitations of proton beam range verification with offline PET/CT scans *Phys. Med. Biol.* **54** 4477
Kooy H M, Rosenthal S J, Engelsman M, Mazal A, Slopsema R L, Paganetti H and Flanz J B 2005 The prediction of output factors for spread-out proton Bragg peak fields in clinical practice *Phys. Med. Biol.* **50** 5847
Krimmer J, Dauvergne D, Létang J M and Testa É 2018 Prompt-gamma monitoring in hadrontherapy: a review *Nucl. Instrum. Methods Phys. Res.* A **878** 58–73
Masiakowski J T, Horton J L and Peters L J 1992 Gadolinium neutron capture therapy for brain tumors: a computer study *Med. Phys.* **19** 1277–84
Morris P A, Aspden R S, Bell J E, Boyd R W and Padgett M J 2015 Imaging with a small number of photons *Nat. Commun.* **6** 5913
Morrison D E, Aitken J B, de Jonge M D, Ioppolo J A, Harris H H and Rendina L M 2014 High mitochondrial accumulation of new gadolinium (III) agents within tumour cells *Chem. Commun.* **50** 2252–4
Moyers M F, Benton E R, Ghebremedhin A and Coutrakon G 2008 Leakage and scatter radiation from a double scattering based proton beamline *Med. Phys.* **35** 128–44
Paganetti H (ed)2018 *Proton Therapy Physics* (Boca Raton, FL: CRC Press)
Paganetti H 2012 Range uncertainties in proton therapy and the role of Monte Carlo simulations *Phys. Med. Biol.* **57** R99
Parodi K *et al* 2007 Patient study of *in vivo* verification of beam delivery and range, using positron emission tomography and computed tomography imaging after proton therapy *Int. J. Radiat. Oncol. Biol. Phys.* **68** 920–34
Polf J C and Newhauser W D 2005 Calculations of neutron dose equivalent exposures from range-modulated proton therapy beams *Phys. Med. Biol.* **50** 3859
Polf J C, Peterson S, McCleskey M, Roeder B T, Spiridon A, Beddar S and Trache L 2009 Measurement and calculation of characteristic prompt gamma ray spectra emitted during proton irradiation *Phys. Med. Biol.* **54** N519
Prusator M T, Ahmad S and Chen Y 2018 Shielding verification and neutron dose evaluation of the Mevion S250 proton therapy unit *J. Appl. Clin. Med. Phys.* **19** 305–10
Safavi-Naeini M, Chacon A, Guatelli S, Franklin D R, Bambery K, Gregoire M C and Rosenfeld A 2018 Opportunistic dose amplification for proton and carbon ion therapy via capture of internally generated thermal neutrons *Sci. Rep.* **8** 16257
Shih J L A and Brugger R M 1992 Gadolinium as a neutron capture therapy agent *Med. Phys.* **19** 733–44
Taguchi K and Iwanczyk J S 2013 Vision 20/20: single photon counting x-ray detectors in medical imaging *Med. Phys.* **40** 3957–69
Verburg J M and Seco J 2014 Proton range verification through prompt gamma-ray spectroscopy *Phys. Med. Biol.* **59** 7089
Wronski M M, Zhao W, Reznik A, Tanioka K, DeCrescenzo G and Rowlands J A 2010 A solid-state amorphous selenium avalanche technology for low photon flux imaging applications *Med. Phys.* **37** 4982–5
Yang M, Virshup G, Clayton J, Zhu X R, Mohan R and Dong L 2010 Theoretical variance analysis of single-and dual-energy computed tomography methods for calculating proton stopping power ratios of biological tissues *Phys. Med. Biol.* **55** 1343
Zheng Y, Newhauser W, Fontenot J, Taddei P and Mohan R 2007 Monte Carlo study of neutron dose equivalent during passive scattering proton therapy *Phys. Med. Biol.* **52** 4481
Zhu Z and Pang S 2018 Few-photon computed x-ray imaging *Appl. Phys. Lett.* **113** 231109